catalysts

MDPI

Article

PtM/CNT (M = Mo, Ni, CoCr) Electrocatalysts with Reduced Platinum Content for Anodic Hydrogen Oxidation and Cathodic Oxygen Reduction in Alkaline Electrolytes

Inna Vernigor, Vera Bogdanovskaya *, Marina Radina, Vladimir Andreev and Oleg Grafov

A.N. Frumkin Institute of Physical Chemistry and Electrochemistry, Russian Academy of Sciences, 119071 Moscow, Russia

* Correspondence: bogd@elchem.ac.ru

Abstract: Bimetallic catalysts containing platinum and transition metals (PtM, M = Mo, Ni, CoCr) were synthesized on carbon nanotubes (CNTs) functionalized in an alkaline medium. Their platinum content is 10–15% by mass. PtM/CNT_{NaOH} are active in both the hydrogen oxidation reaction (HOR) and the oxygen reduction reaction (ORR) in alkaline electrolytes. Although catalysts based on a single transition metal are inactive in the HOR, their activity in the cathode process of ORR increases relative to CNT_{NaOH}. When using the rotating ring-disk electrode method for ORR, PtM/CNT showed a high selectivity in reducing oxygen directly to water. In HOR, the PtM/CNT catalyst had an activity comparable to that of a commercial monoplatinum catalyst. The results obtained show that it is possible to use the PtM/CNT catalyst in an alkaline fuel cell both as an anode and as a cathode.

Keywords: bimetallic catalyst; carbon nanotubes (CNT); hydrogen electrooxidation; oxygen electroreduction; alkaline electrolyte

Citation: Vernigor, I.; Bogdanovskaya, V.; Radina, M.; Andreev, V.; Grafov, O. PtM/CNT (M = Mo, Ni, CoCr) Electrocatalysts with Reduced Platinum Content for Anodic Hydrogen Oxidation and Cathodic Oxygen Reduction in Alkaline Electrolytes. *Catalysts* **2023**, *13*, 161. https://doi.org/10.3390/catal13010161

Academic Editors: Vladimir Guterman, Sergey Belenov and Anastasia Alekseenko

Received: 9 December 2022
Revised: 27 December 2022
Accepted: 5 January 2023
Published: 10 January 2023

1. Introduction

The ever-increasing consumption of fossil fuels, accompanied by climate change and environmental pollution, calls for the development of efficient, environmentally friendly, and sustainable energy sources [1,2]. A fuel cell (FC), where the chemical energy of the fuel is directly converted into electrical energy through two electrochemical reactions, namely a hydrogen oxidation reaction (HOR) at the anode and an oxygen reduction reaction (ORR) at the cathode, comprises one of the most promising devices that meet these requirements [3].

At present, research is mainly focused on the development of cathode electrocatalysts, since the kinetics of cathodic ORR is much slower than that of anodic HOR; in other words, the FC voltage drop is generally associated with the overvoltage of the cathode reaction [4,5]. A wider range of catalysts, including catalytic systems without platinum, can be used in alkaline electrolytes. It was shown [6–10] that CNTs subjected to functionalization and nitrogen doping have activity close to platinum in ORR. While in the HOR reaction, platinum-free catalysts in an alkaline medium have low activity; thus, as a rule, a high platinum content is required for its implementation [11]. The hydrogen oxidation reaction in an alkaline medium is described by the following equation [12]:

$$H_2 + 2OH^- \rightarrow 2H_2O + 2e^- \quad (1)$$

At least two pathways of HOR in alkaline media are considered: the Tafel–Volmer and Heyrovský–Volmer mechanisms [12]. According to the first path, the dissociative adsorption of H_2 avoiding electron transfer (chemical) proceeds at the first stage, leading to the formation of two adsorbed hydrogen atoms on the electrode surface. According to the Heyrovský–Volmer mechanism, the first stage involves the electrochemical dissociative adsorption of the H_2 molecule and electron transfer from the molecular H_2 to the catalyst.

As a result, an adsorbed hydrogen atom on the electrode surface, a water molecule, and one electron are formed.

$$H_2 + OH^- \rightarrow H_{ad} + H_2O + e^- \quad (2)$$

At the next stage, the hydrogen atom combines with OH^- to form water and one electron:

$$H_{ad} + OH^- \rightarrow H_2O + e^- \quad (3)$$

Classically, the HOR mechanism can be assessed by the Tafel slope obtained from the polarization curve [13]. This analysis reveals the internal nature of an electrocatalytic material, while the empirical value of the Tafel slope can help to determine possible mechanisms on the surface of the material [13]. Since OH^- species occurring in the Heyrovský and Volmer stages still hinder the fundamental understanding of the mechanism of HOR, disagreements about the role of OH^- in HOR exist to the present day [12]. Several kinetic descriptors were proposed in order to improve the activity of HER/HOR in an alkaline medium [14]. Among them, the most discussed are the hydrogen binding energy (HBE) and the surface oxophilicity [15]. The ability to adsorb and dissociate the molecule H_2, being a necessary, however, insufficient criterion for HOR catalysts, fails to provide a deep understanding of the nature of electrocatalyst activity. Therefore, it was assumed [16] that surface oxophilicity comprises an equally important descriptor of HOR kinetics. It was shown that combining Pt with more oxophilic metals (for example, Ru, Ni, Ir) enhances the interaction of the catalyst with H_2O/OH^-, which leads to an increase in the activity of HOR in an alkaline medium [16]. It was established [17] that doping with Mo leads to an increase in both the catalytic activity and stability of Pt in the hydrogen oxidation reaction in FC. Molybdenum was selected as the second metal since it is one of the few available elements that act as a "source" of electrons [18]. In addition, the high hydrogen-Mo bond strength (72 kcal/mol) significantly exceeds that of nickel and cobalt (48 kcal/mol). It can be assumed that, when combined with platinum, these metals will have a different effect on the activity in the hydrogen oxidation reaction. Although the catalytic activity of catalysts based on Pt-Mo alloys in ORR has been studied to a lesser extent [18], the catalytic activity of catalysts based on Pt-Mo alloys in ORR has been determined [19]. Here, the PtMo/CNT catalyst exhibited activity comparable to that of the Pt/CNT catalyst. Conversely, the bimetallic catalysts, including nickel [20–22] and cobalt [23–25], are known as electrocatalysts for the oxygen reduction reaction. It was shown that in an acidic electrolyte, the activity of bimetallic PtNi/C [21,22] and PtCo/C catalysts [24–26] and their ternary alloys [27] exceeds that of the monometallic Pt/C platinum catalyst. Despite certain advantages of fuel cells using an alkaline electrolyte over those using an acidic electrolyte [28], the largest number of publications have been devoted to studying bimetallic systems for ORR and HOR in an acidic medium. For this reason, this work focused on investigating electrocatalysts having no Pt or reduced Pt content for alkaline media.

Most electrocatalysts described in the literature are designed for only one of the two reactions. Here, bi- and tri-metallic catalysts PtM (M = Mo, Ni, CoCr), as well as monometallic systems based on transition metals synthesized on CNTs, were studied in the hydrogen oxidation and oxygen reduction reactions in alkaline electrolytes in order to reveal the role of the second metal in both anodic and cathodic reactions.

2. Results and Discussion

Figure 1 presents cyclic current-voltage curves (CV) recorded to assess the state of the electrochemically active surface.

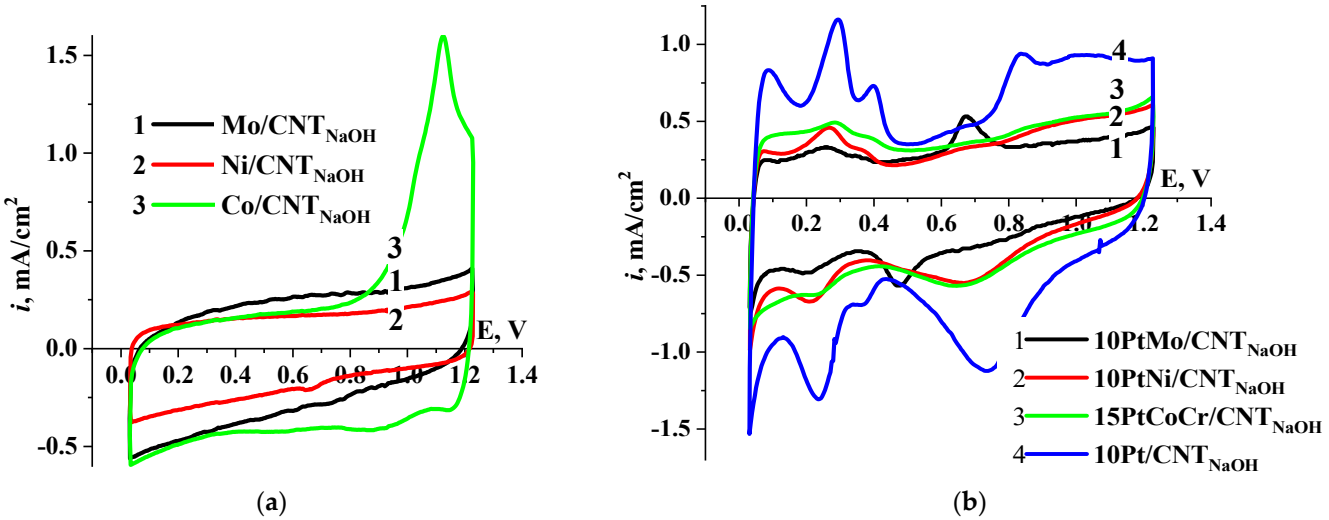

Figure 1. (**a**) CV for catalysts containing transition metals (shown in Figure); (**b**) CV for catalysts containing platinum (shown in Figure); 0.1 M KOH, 0.05 mV/s, m_{cat} = 0.15 mg/cm^2.

Among the catalysts based on transition metals, only Co/CNT_{NaOH} is characterized by a maximum in the potential range (1.0–1.2 V).

On the CV obtained for bimetallic catalysts, the maxima of hydrogen adsorption and desorption are smoothed compared to those for the Pt/CNT_{NaOH} catalyst (Figure 1b, curve 4), although the platinum content in the bulk PtM/CNT_{NaOH} (M = Mo, Ni, CoCr) and Pt/CNT_{NaOH} catalysts is identical (10–15 wt%). However, according to the XPS, platinum content varies over the surface (Table 1), indicating that the platinum surface is partially covered with transition metal nanoparticles and/or their oxides. As a result, $S_{EAS\,Pt}$ for PtMo/CNT_{NaOH} amounts to 35 m^2/g, for PtNi/CNT_{NaOH}—41.2 m^2/g, and, for PtCoCr/CNT_{NaOH}—32.3 m^2/g, while for Pt/CNT_{NaOH} $S_{EAS\,Pt}$ amounts to 61.9 m^2/g (Figure 1b). In addition, for PtMo/CNT_{NaOH}, a redox maximum is observed at 0.7 V on the anodic and at 0.5 V on the cathodic course, which can be attributed to the redox transformations of molybdenum Mo^{n+}/Mo^0. SEM images and elemental composition of the PtMo/CNT_{NaOH} and PtNi/CNT_{NaOH} catalysts are shown in Figure S1. According to the presented data, the catalysts are characterized by a uniform distribution of metals on the surface and almost complete coverage of the carbon substrate.

Table 1. Surface composition (XPS, at %) of studied catalysts.

Catalyst	C1s	O1s	Pt4f	Ni2p	Mo3d	Co3d	Cr2p
	at%						
10Pt/CNT_{NaOH}	94.69	2.46	2.18				
10PtNi/CNT_{NaOH}	96.8	2.21	0.63	0.36			
10PtMo/CNT_{NaOH}	96.66	2.81	0.36		0.16		
15PtCoCr/CNT_{NaOH}	89.67	6.69	1.63			0.74	1.27

Figure 2 shows the XPS spectra of PtMo/CNT_{NaOH} as an example, where, in the PtMo catalyst on the CNT surface, platinum can be found predominantly in the metallic state (Pt^0 (71.3 eV)). This may be attributed to the highly negative redox potential of the Mo^{3+}/Mo^0 pair since, in the studied catalyst, molybdenum, occurs in the MoO_3 oxide state. XPS spectra for the PtNi/CNT_{NaOH} catalyst are shown in Figure S2. This catalyst is also characterized by the presence of the nickel oxide phase Ni_2O_3. A detailed discussion of XPS spectra is given in Figure S2.

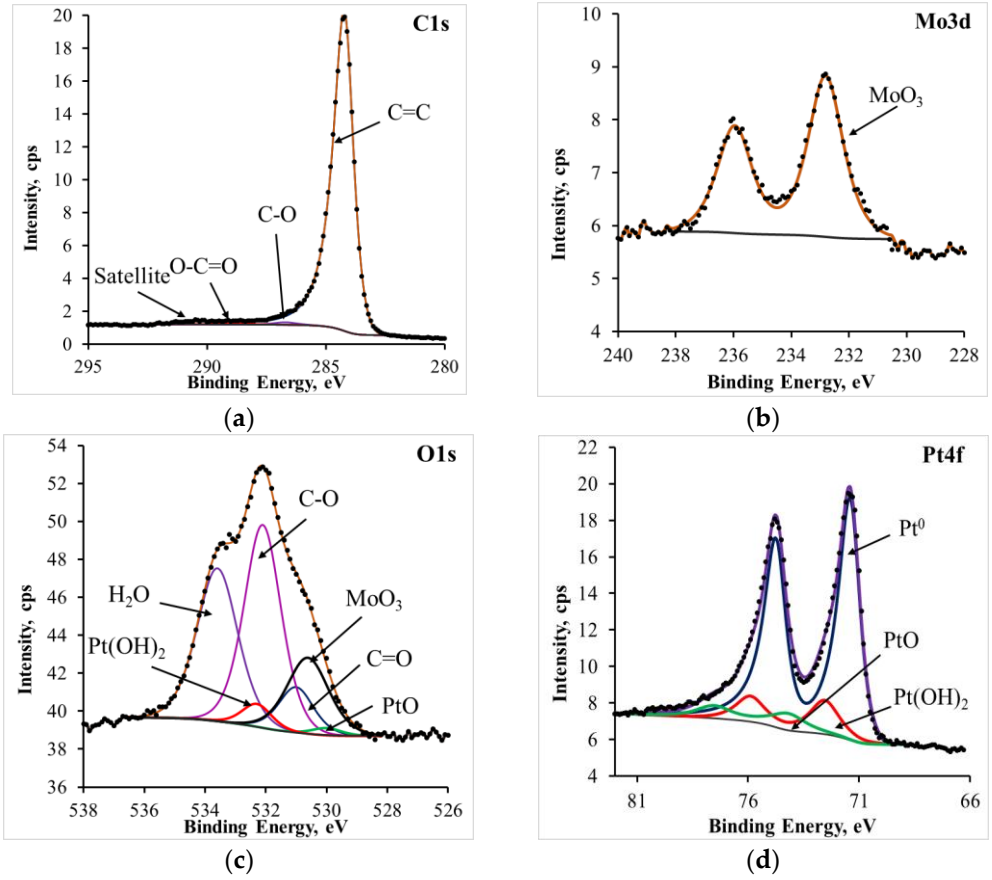

Figure 2. C1s (**a**), Mo3d (**b**), O1s (**c**), and Pt4f (**d**) X-ray spectra recorded on PtMo/CNT_{NaOH}.

2.1. Hydrogen Electrooxidation Reaction

Figure 3 shows the polarization curves of hydrogen oxidation obtained for various catalysts. Catalysts based on transition metals Mo, Ni, and Co, containing no platinum, are inactive in HOR. However, bimetallic catalysts are characterized by a higher value of the limiting diffusion current. Some deviation in the value of the limiting currents from the calculated value of the limiting diffusion current can be associated with a significant thickness of the dispersed catalyst layer that appears on the disk electrode. At the same catalyst mass (0.150 mg/cm^2), the densities of the materials differ, which affects the layer thickness and current values. A comparison of the values of the limiting current of monoplatinum catalysts shows that the theoretically calculated value of the limiting diffusion current is achieved on a commercial catalyst with 40 wt% Pt, since the layer thickness, in this case, is much less when using a catalyst with 10Pt/CNT_{NaOH}. At the same time, the mass activity of 40 Pt/C systems is three times less (Table 2). The density of bimetallic systems with an equal content of platinum depends on the molecular weight of the transition metal: 95.9-Mo; 58.9-Co; 58.7-Ni. Current values at 0.4 V are presented in Table 2. It can be seen that the current closest to the limiting diffusion current at 0.4 V is observed on the 10 PtNi/CNT_{NaOH} catalyst. A more detailed discussion of the observed dependences requires additional measurements to take into account the effect of their composition and structure on the characteristics of catalysts.

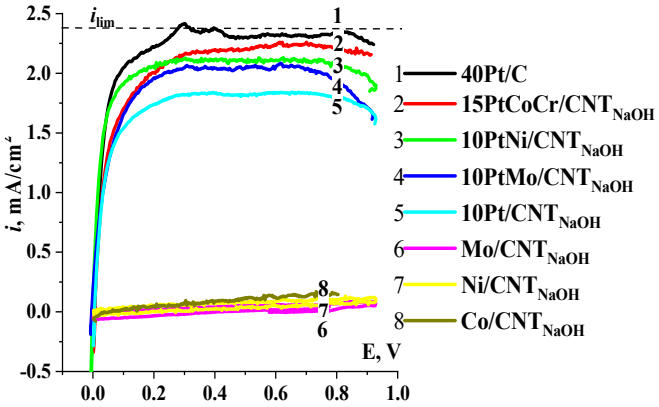

Figure 3. Polarization curves of hydrogen oxidation in 0.1M KOH. 0.005 V/s; 1500 rpm; m_{cat} = 0.15 mg/cm^2.

Table 2. Electrochemical parameters of HOR.

Catalyst	i_{dif}, mA/cm^2	$j_{mass} \times 10^3$, mA/mg Pt	η, V
	at 0.4 V		at 1.5 mA/cm^2 (1500 rpm)
40Pt/C	2.31	36.2	0.037
10Pt/CNT$_{NaOH}$	1.82	114.6	0.088
10PtMo/CNT$_{NaOH}$	2.05	128.8	0.066
10PtNi/CNT$_{NaOH}$	2.11	132.9	0.035
15PtCoCr/CNT$_{NaOH}$	2.18	91.6	0.076

The limiting current of PtMo, PtNi, and PtCoCr approach that of the commercial catalyst 40 Pt/C (Figure 3). The calculated mass activities (j_{mass}) for the studied catalysts are characterized by higher values, confirming the positive effect of the transition metal on the activity of platinum in the hydrogen oxidation reaction.

The limiting diffusion current was determined using the Levich equation:

$$i_{dif} = 0.62nFD^{2/3}\, v^{-1/6}\, w^{1/2}C_{H2}, \quad (4)$$

where n—number of electrons involved in the reduction of one O_2 molecule, F—Faraday constant (96,485 C/mol), D—diffusion coefficient of the active substance in the electrolyte (3.4×10^{-5} m^2/s), v—kinematic viscosity of the electrolyte (0.1M KOH—0.905×10^{-2} m^2/s), ω—rotational speed of the electrode (rad/s), and C_{H2}—solubility of molecular hydrogen in 0.1 M KOH (0.7×10^{-6} mol/m^3) [29]. Its value amounted to 2.4 mA/cm^2.

The dependence of the limiting current on the square root of the rotational speed of the electrode (Figure 4c) is described by a straight-line correlation, starting at the origin. This indicates that the observed limiting current comprises the hydrogen-scale limiting diffusion current. As shown in several works [11–13], using formal electrochemical kinetics in some cases helps to identify the stage-limiting electrode reaction. The Tafel dependences plotted in the initial range of potentials (steady potential) characterize the kinetics, excluding concentration polarization. As shown in Figure 4a, a potential region can be distinguished in the range of the Tafel dependence, where the slope of the Tafel curve equals 0.120 V, describing the stage of a delayed transfer of the first electron. The article [16] discussed the role of the oxophilicity of the second metal in bimetallic systems, where the greatest effect in these conditions was provided by Ni. Analysis of the data obtained in this work and a comparison of the effect on the reactivity of platinum in bimetallic catalysts showed that nickel and cobalt have the greatest influence on HOR. In terms of hydrogen oxidation, however, the corresponding mono-metallic catalysts are inactive, being practically identical to Mo (Figure 3, curves 6–8). The higher stability of bimetallic PtNi and PtCo systems is

confirmed by current transients (Figure 4b). It should be noted that the activity of a monometallic platinum catalyst having a platinum content of 10 wt% is inferior to all bimetallic samples, which indicates a synergistic effect in the presence of a second metal. Since the binding energy with the hydrogen of Pt equals 65 kcal/mol, along with 48 kcal/mol for Ni and Co and 72 kcal/mol for Mo [30], it can be assumed that an electron transfer scheme from the adsorbed hydrogen molecule, which further dissociates, occurs for the first two metals. The adsorbed hydrogen molecule can dissociate on bimetallic systems having high bond strength, with the electron being further transferred from the hydrogen atom. This assumption requires additional research related to the role of the OH^- ions in the mechanism of the hydrogen oxidation reaction.

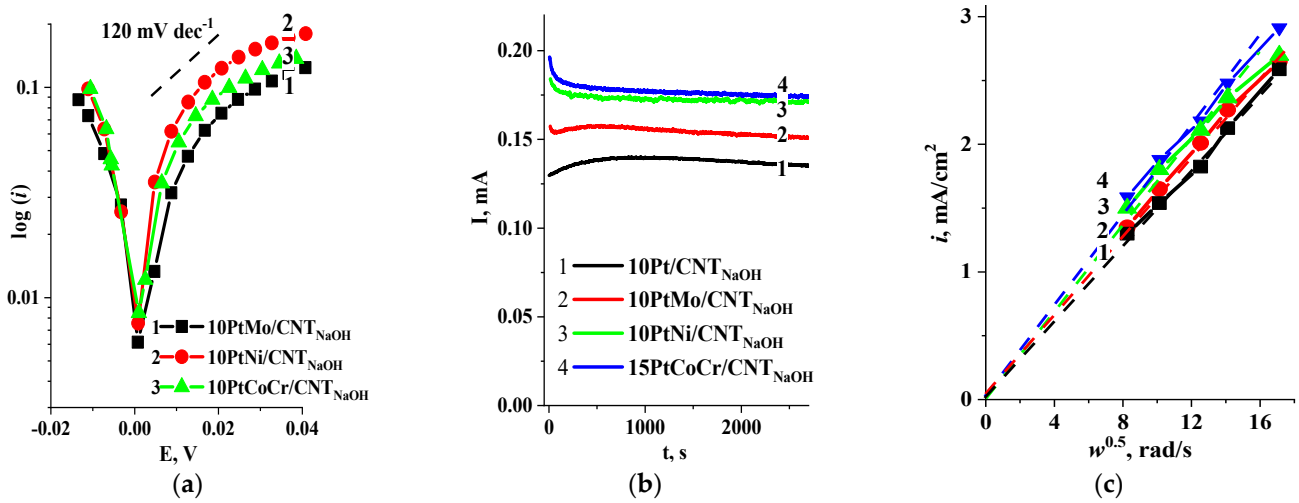

Figure 4. (**a**) Polarization curves in Tafel coordinates for platinum-modified materials (indicated in Figure), O_2, 0.1 M KOH, 5 mV/s, 1500 rpm; (**b**) Chronoamperometric measurements at 0.4 V, 650 rpm; (**c**) Limiting current as a function of electrode rotation speed.

2.2. Oxygen Reduction Reaction

Figure 5 presents the polarization curves of oxygen reduction on all the studied systems in an alkaline electrolyte. When nanoparticles of transition metals are deposited on the surface of functionalized CNTs, their activity in ORR increases. Among the catalysts based on transition metals, Mo/CNT_{NaOH} is characterized by the most positive onset potential of oxygen reduction and the half-wave potential. The combination of transition metal and platinum nanoparticles contributes to a further increase in the activity in ORR. Although Ni/CNT_{NaOH} is characterized by the lowest value of $E_{1/2}$ = 0.7 V, the $PtNi/CNT_{NaOH}$ catalyst exhibits the highest activity among bimetallic systems (Table 3).

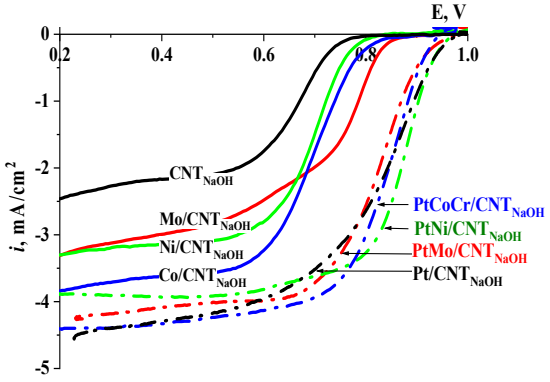

Figure 5. Polarization curves on studied catalysts in 0.1 M KOH; O_2; 0.005 mV/s; m_{cat} = 0.15 mg/cm^2, w = 1500 rpm.

Table 3. Electrochemical parameters of ORR.

Catalyst	$E_{1/2}$, V	i_{kin}, mA/cm^2 at 0.9 V	n//% HO_2^- at 0.5 V
CNT_{NaOH}	0.66	-	-
Mo/CNT_{NaOH}	0.76	-	-
Ni/CNT_{NaOH}	0.70	-	-
Co/CNT_{NaOH}	0.71	-	-
$10Pt/CNT_{NaOH}$	0.84	0.88	3.42//28.9
$10PtMo/CNT_{NaOH}$	0.83	0.49	3.59//20.0
$10PtNi/CNT_{NaOH}$	0.87	1.07	3.78//10.8
$15PtCoCr/CNT_{NaOH}$	0.84	0.61	3.68//15.8

Tafel plot has proved another way to analyze the electrocatalytic activity and reaction mechanism of electrocatalysts. The curves corresponding to monometallic catalysts containing one transition metal are shifted to more positive potentials relative to the initial CNTs. The values of the Tafel slopes for monometallic catalysts are presented in a narrow potential range of ~15 mV and range from 85 to 70 mV/decade of current, that is, they are close to each other. The current value is slightly higher on Mo/CNT_{NaOH}, which is probably due to differences in the values of the electrochemically active surface of monometallic catalysts. This can be seen from Figure 1a. The larger the S_{EAS} value on the CV the greater the current density on the polarization curve in the ORR (Figure 5), as well as Figure S3, presented in Tafel coordinates. Therefore, the activity of monometallic catalysts in ORR weakly depends on the nature of the metal. However, a more detailed assessment of the role of the metal in this case requires additional studies and is beyond the scope of this work.

Two different linear Tafel slopes were noticed at low and higher overpotentials for bi- and tri-metal catalysts. Tafel slope 110–120 mV dec-1 indicates that the transfer of the first electron is the rate-limiting step.

For a more detailed study of the mechanism of oxygen reduction on the above bimetallic catalysts, the RRDE method was used, which allows the intermediate product of oxygen reduction, namely hydrogen peroxide (HO_2^- in an alkaline electrolyte) to be quantified, since simultaneous measurement of currents on the disk and ring electrodes depending on the potential on the disk can be carried out [31]. Figure 6 shows the polarization curves of oxygen reduction on a disk electrode having applied catalysts and the corresponding curves of hydrogen peroxide oxidation on a ring electrode at different rotational speeds of the electrode. It can be seen that the oxidation of peroxide occurs at significantly lower positive potentials than that of the commencement of oxygen reduction. Thus, in the kinetic region (1.0–0.8 V), oxygen is reduced directly to water, via a four-electron path. When the value of ~0.8 V is reached, the current on the ring increases, which corresponds to the formation of hydrogen peroxide. At a potential of 0.8 V, CNTs, being carriers of metal nanoparticles, become active in ORR. An increase in the current at the ring electrode is associated with an increased contribution of oxygen reduction on the CNT surface to the total ORR current.

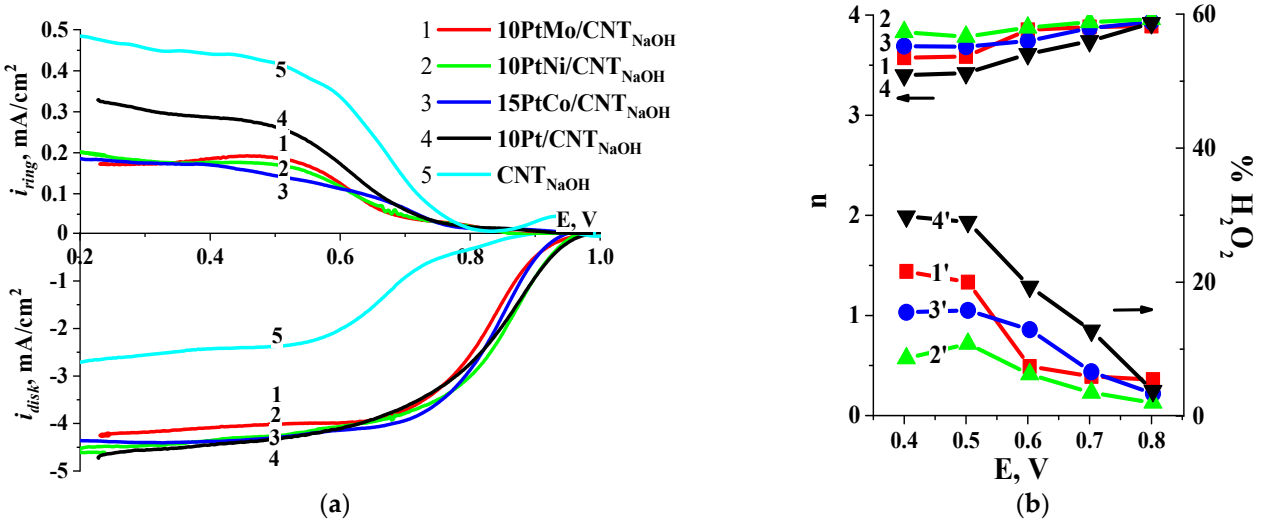

Figure 6. (**a**) Reduction polarization curves of O_2 on a disk electrode and their corresponding HO_2^- oxidation curves on the ring electrode, 0.1 M KOH, 100 mcg/cm^2, 5 mV/s, 1500 rpm, E_{ring} = 1.2 V; (**b**) Dependence of the number of electrons (n) involved in the reaction (1, 2, 3, 4) and yield of hydrogen peroxide (1′, 2′, 3′, 4′) on the electrode potential.

The oxidation current of hydrogen peroxide at the ring electrode for PtM/CNT$_{NaOH}$ (M=Mo, Ni, Co) is less than that for the mono-metallic platinum catalyst (Figure 6a). At 0.5 V, the number of electrons involved in the reaction amounts to 3.78 for PtNi/CNT$_{NaOH}$ and 3.42 for Pt/CNT$_{NaOH}$, while the yield of hydrogen peroxide reaches 28.9% and 10.8%, respectively. This may be due to the fact that, in the Pt/CNT$_{NaOH}$, the ratio of the surface of a metal phase to the CNT surface is less than that for the PtM/CNT$_{NaOH}$ catalysts, leading to the formation of more hydrogen peroxide. The activity in ORR and the binding energy of metals with oxygen increases in the series of Mo (−1.6 eV), Co (−0.05 eV), Ni (0.04 eV), and Pt (1.5 eV). This series is in agreement with the results obtained for bimetallic catalysts, where PtNi/CNT$_{NaOH}$ is most active, followed by PtCoCrCNT$_{NaOH}$ and PtMo/CNT$_{NaOH}$, while the activity of all bimetallic catalysts exceeds that of Pt/CNT$_{NaOH}$, which may indicate a synergistic effect of increasing activity in ORR. PtNi/CNT$_{NaOH}$ exhibits the highest activity in both HOR and ORR, which can be explained by the close electronic configuration of Pt and Ni atoms, since they contain 8 electrons at the external energy level (5d and 3d, for Pt and Ni, respectively).

The dependence of the number of electrons (*n*) and the yield of hydrogen peroxide on the electrode potential is shown in Figure 6b. It can be seen that, with increasing polarization, the number of electrons involved in the reaction decreases (curves 1–4), while the yield of hydrogen peroxide increases (curves 1′–4′). This indicates that, at potentials below 0.8 V, the total oxygen reduction current includes that of a two-electron reduction of O_2 to hydrogen peroxide on a platinum-free carrier surface.

2.3. Corrosion Stability Study

The most important characteristic of electrocatalysts is their stability. Figure S4 shows a diagram of the relative decrease in S_{Pt} during cycling. Platinum and transition metal based catalysts have improved corrosion resistance compared to a monoplatinum catalyst. The decrease in the EAS of platinum for bi- and trimetallic systems does not exceed 40%, while for 10Pt/CNT$_{NaOH}$ the surface of platinum decreases by 67% in 100 cycles.

3. Materials and Methods

3.1. Method of Processing CNTs in an Alkaline Solution

The functionalization was carried out by processing the initial CNTs (Nanotechcenter LLC, Tambov, Russia) in 1 M solution of NaOH (Chimmed LLC, Moscow, Russia) at 100 °C

for an hour, followed by washing with deionized water to a neutral pH value. The CNTs were further dried in a vacuum oven at 80 °C until all the moisture was removed. The resulting material was designated as CNT_{NaOH}.

3.2. Synthesis of Mo/CNT_{NaOH}, PtMo/CNT_{NaOH}, Ni/CNT_{NaOH}, PtNi/CNT_{NaOH}, and Co/CNT_{NaOH} Catalysts

In this series, as a rule, ~20 wt% of the metal phase was applied onto CNT_{NaOH}. A water suspension of CNT_{NaOH} was subjected to ultrasonic treatment for 30 min. Subsequently, the required amount of an aqueous salt solution (ammonium molybdate, nickel nitrate, or cobalt acetate (Alfa Aesar, Ward Hill, MA, USA)) and chloroplatinic acid (Aurat, Moscow, Russia) were added to an aqueous CNT suspension under continuous ultrasound treatment. Following 15 min, formic acid was added in an amount sufficient to reduce metals; the mixture was kept for an hour under periodic stirring with subsequent evaporation in a water bath. The dry powder was subjected to heat treatment at 440 °C in an Ar atmosphere for 2 h, followed by cooling to room temperature.

3.3. Synthesis of PtCoCr/CNT_{NaOH}

High-temperature pyrolysis using N_4 complexes of cobalt and chromium as precursors was carried out in order to obtain $PtCoCr/CNT_{NaOH}$. The initial reagents included $H_2PtCl_6 \cdot 6H_2O$ (Aurat, Moscow, Russia), cobalt tetra methoxyphenyl porphyrin (TMPhCo) (Aldrich, Louis, MO, USA), chromium phthalocyanine (PC, synthesized at IPCE RAS, Russia), and cobalt and chromium acetates (Aurat, Moscow, Russia). The weighted quantities of CNT_{NaOH} and organic precursors were dispersed in solvents: CM in ethyl alcohol, PC in chloroform, and TMPhCo in a mixture of chloroform and ethyl alcohol at a ratio of 1:1. Metal salts were dissolved in ethyl alcohol. The resulting suspensions were mixed, followed by the addition of the calculated amount of H_2PtCl_6 in the form of a solution in ethyl alcohol. The resulting mixture was sonicated for 2 h, followed by evaporation in a water bath. The dry powder was ground in a mortar, subjected to pyrolysis in an inert atmosphere at 600 °C for two hours, and cooled to room temperature in an inert gas current.

3.4. Modification of CNT with Platinum Using Polyol Method

The CNT_{NaOH} weighted quantity added to ethylene glycol (ECOS-1 CJSC, Moscow, Russia) was subjected to ultrasonic treatment for 1 h. Further, the CM suspension in ethylene glycol was transferred to a round-bottom flask, which was installed in a glycerin bath, and purged with argon for an hour, followed by heating to 110–130 °C. Here, a solution containing $H_2PtCl_6 \cdot 6H_2O$ was added to ethylene glycol through a drip funnel. The temperature treatment was carried out for 1.5 h under argon barbotage. The resulting mixture was decanted and washed with water; the solid precipitate was separated using a centrifuge and placed in a drying oven.

A number in the catalyst designation (10PtM/CNT_{NaOH}, 40Pt/C) stands for Pt wt% determined using the spectrophotometry (error of ± 2 wt%). In bi- and tri-metallic catalysts, the mass ratio of platinum and metal equaled 1:1.

3.5. Electrochemical Measurements

The experiments were carried out using a three-electrode electrochemical cell with separated electrode spaces. For the rotating disk electrode (RDE) method, a carbositall disk electrode (S_{geom} = 0.126 cm^2) was used as a working electrode. Rotating ring-disk electrode (RRDE) studies were carried out using a carbositall disk electrode ($S_{disk\ geom}$ = 0.196 cm^2) having a platinum ring electrode ($S_{ring\ geom}$ = 0.110 cm^2). Measurements were carried out in a 0.1 M KOH solution (pH 12.7). Hg/HgO was used as a reference electrode. The potential value of this electrode relative to a reversible hydrogen electrode (R.H.E.) was calculated by Equation: $E = E^0 + 0.059\ pH$, which equals 0.865 V. Platinum wire was used as a counter electrode.

To prepare catalyst ink, 2 mg of catalyst was dispersed in 500 µL of isopropyl alcohol; 5 µL (~150 µg/cm^2) of this suspension was applied to the surface of the working electrode using a micropipette. Samples were air-dried at room temperature for ~30 min.

Cyclic current-voltage curves (CV) were recorded using a stationary electrode in an Ar atmosphere at a scan rate of 0.05 V/s. The electrochemically active Pt surface (S_{EAS}) was determined by integrating the charge on the CV spent for hydrogen desorption, assuming that 0.210 µL/cm^2 is necessary to fill a hydrogen monolayer in 1 cm^2 of the Pt surface.

In order to determine the activity of the studied materials in the HOR, the polarization curves were recorded in an electrolyte saturated with H_2. The scan rate equaled 0.005 V/s at an electrode rotation rate of 650 to 2800 rpm. The catalytic activity was determined on the basis of the values of the maximum diffusion current density (i_{lim}, mA/cm^2). The current transients of HOR were recorded using an RDE (650 rpm) at 0.4 V.

Prior to commencing the measurements using the RRDE, disk and ring electrodes were activated independently by cycling the potential in the range of 0.05–1.20 V in an argon-deaerated electrolyte. The ring electrode was platinized in 2–3% $H_2PtCl_6 \cdot 6H_2O$ in 0.5 M solution H_2SO_4 under galvanostatic mode (1 mA/cm^2). The roughness coefficient of the platinized ring was determined using the surface area calculated from the CV for the hydrogen desorption region. The roughness coefficient amounted to 80–90. The transfer efficiency coefficient N of the product of oxygen reduction, i.e., OH_2^-, from the disk electrode to the ring electrode was determined from the geometric dimensions of the two electrodes and amounted to 0.286.

Activity (half-wave potential ($E_{1/2}$, V) and current density in the kinetic region of potentials (i_{kin}, A/cm^2)) of the studied materials were evaluated by polarization curves obtained for a disk electrode during ORR in an oxygen-saturated electrolyte at different rotational speeds of the electrode. The scan rate was 0.005 V/s. The potential of the ring electrode was maintained at 1.2 V. On the basis of the polarization curves for the disk and ring electrodes, the number of electrons n participating in the reaction and the yield of hydrogen peroxide were also calculated using the Formulas:

$$n = \frac{4I_d \times N}{I_d N + I_r} \quad (5)$$

$$\%H_2O_2 = 100 \times \frac{2I_r}{I_d N + I_r} \quad (6)$$

where, I_d—current on the disc electrode, I_r—current on the ring electrode, and N—transfer efficiency coefficient.

3.6. Determination of Stability

The corrosion resistance of the catalytic systems was determined by an accelerated corrosion test. The method involves cycling the electrode potential in the range of 0.6–1.3 V (R.H.E.), i.e., in the absence of a depolarizer (oxygen) in an electrolyte solution (0.1 M KOH), at a rate of 100 mV/s for 1000 cycles. Following 100, 500, and 1000 cycles, S_{EAS} was determined using CV in the argon atmosphere, along with defining the activity in the ORR using polarization curves in an oxygen-saturated solution.

3.7. Determination of Platinum Content in Synthesized Catalysts

The method involves measuring the optical density of a solution containing the Pt complex of divalent tin chloride ($SnCl_2$)) over a wide range of Pt concentrations, from 0.4 to 100 µg Pt·mL^{-1}. The optical density of the test solution was measured using a SPECORD M40 spectrophotometer. A more detailed description of the procedure is presented elsewhere [32].

3.8. X-ray Photoelectron Spectroscopy (XPS)

X-ray photoelectron spectroscopy (XPS) studies were performed using an OMICRON ESCA + spectrometer (Germany) with an aluminum anode equipped with an AlKα XM1000 monochromatic X-ray source (with an emission energy of 1486.6 eV and a power of 252 W). A CN-10 charge neutralizer with an emission current of 4 μA and a beam energy of 1 eV was used to eliminate the local charge on the analyzed surface. The transmittance energy of the analyzer was 20 eV for the high resolution spectra of single elements. Fluctuation of the peak positions did not exceed ±0.2 eV.

3.9. Scanning Electron Spectroscopy and EDX Analysis

SEM images and elemental content (EDX) were obtained using a JED-2300 Analysis-Station JEOL scanning electron microscope.

4. Conclusions

Catalysts based on Mo, Ni, and CoCr transition metals and PtMo, PtNi, and PtCoCr on CNT_{NaOH} with reduced platinum content (10–15 wt%) were investigated in the hydrogen electrooxidation and oxygen electroreduction reactions in an alkaline electrolyte. It was shown that catalysts based on a single transition metal are inactive in the HOR; in the ORR, however, their activity increases significantly relative to that of the CNT_{NaOH}. Mo/CNT_{NaOH} showed the greatest activity among the mono-metallic catalysts. The half-wave potential for this catalyst amounted to 0.76 V.

It was established that catalysts containing Pt are characterized by high activity in the HOR. Here, the mass activity of the synthesized catalysts exceeded this value for a commercial Pt/C catalyst having 40 wt% of platinum. In ORR, the studied catalysts exhibit selectivity toward direct water formation during the reduction of oxygen. When using the catalysts containing a transition metal, the yield of hydrogen peroxide was lower than that obtained on Pt/CNT_{NaOH}. The highest number of electrons involved in the reaction observed for $PtNi/CNT_{NaOH}$ amounted to 3.78 (at 0.5 V).

Thus, alloying Pt with a transition metal proved an effective method for reducing the content of expensive platinum while maintaining high stability and catalytic activity in both HOR and ORR in an alkaline electrolyte.

Supplementary Materials: The following are available online at https://www.mdpi.com/article/10.3390/catal13010161/s1, Figure S1: SEM image and elemental composition (EDX) of synthesized catalysts, Figure S2: C1s (a), Ni2p3/2 (b), O1s (c), and Pt4f (d) X-ray spectra recorded on $10PtNi/CNT_{NaOH}$, Figure S3: Tafel plots for a—transition metal catalysts, b—Pt-containing catalysts, Figure S4: Diagrams of changes in the relative size of the surface of platinum during accelerated corrosion testing. 0.1M KOH, 50 mV/s, 100 $\mu g/cm^2$.

Author Contributions: Conceptualization, project administration, data curation, V.B.; investigation, methodology, electrochemical measurements, I.V. and M.R.; supervision, data curation, V.A.; X-ray spectra preparation, O.G. All authors have read and agreed to the published version of the manuscript.

Funding: This research was funded by RFBR project BRICS_T No.19-53-80033.

Data Availability Statement: Additional data are available upon request from the corresponding author.

Conflicts of Interest: The authors declare no conflict of interest.

References

1. Barbir, F. *PEM Fuel Cells: Theory and Practice*, 2nd ed.; Elsevier, Inc.: Amsterdam, The Netherlands, 2013.
2. Zaman, S.; Huang, L.; Douka, A.I.; Yang, H.; You, B.; Xia, B.Y. Oxygen Reduction Electrocatalysts toward Practical Fuel Cells: Progress and Perspectives. Angew. *Chem. Int. Ed.* **2021**, *60*, 17832. [CrossRef]
3. Jacobson, M.Z.; Colella, W.G.; Golden, D.M. Cleaning the air and improving health with hydrogen fuel-cell vehicles. *Science* **2005**, *308*, 1901–1905. [CrossRef]

4. Li, Y.; Li, Q.; Wang, H.; Zhang, L.; Wilkinson, D.P.; Zhang, J. Recent Progresses in Oxygen Reduction Reaction Electrocatalysts for Electrochemical Energy Applications. *Electrochem. Energy Rev.* **2019**, *2*, 518–538. [CrossRef]
5. Talukder, N.; Wang, Y.; Nunna, B.B.; Lee, E.S. An In-Depth Exploration of the Electrochemical Oxygen Reduction Reaction (ORR) Phenomenon on Carbon-Based Catalysts in Alkaline and Acidic Mediums. *Catalysts* **2022**, *12*, 791. [CrossRef]
6. Qian, Z.; Sun, B.; Du, L.; Lou, S.; Du, C.; Zuo, P.; Ma, Y.; Cheng, X.; Gao, Y.; Yin, G. Insights into the role of oxygen functional groups and defects in the rechargeable nonaqueous Li–O_2 batteries. *ElectrochimicaActa* **2018**, *292*, 838–845. [CrossRef]
7. Bogdanovskaya, V.; Vernigor, I.; Radina, M.; Sobolev, V.; Andreev, V.; Nikolskaya, N. Modified Carbon Nanotubes: Surface Properties and Activity in Oxygen Reduction Reaction. *Catalysts* **2021**, *11*, 1354. [CrossRef]
8. Bogdanovskaya, V.; Vernigor, I.; Radina, M.; Andreev, V.; Korchagin, O.; Novikov, V. Carbon Nanotube Modified by (O, N, P) Atoms as Effective Catalysts for Electroreduction of Oxygen in Alkaline Media. *Catalysts* **2020**, *10*, 892. [CrossRef]
9. Hu, C.; Dai, L. Doping of carbon materials for metal-free electrocatalysis. *Adv. Mater.* **2019**, *31*, 1804672.
10. Zhang, X.; Zhang, X.; Zhao, S.; Wang, Y.Q.; Lin, X.; Tian, Z.Q.; Shen, P.K.; Jiang, S.P. Precursor modulated active sites of nitrogen doped graphene-based carbon catalysts via one-step pyrolysis method for the enhanced oxygen reduction reaction. *Electrochimica Acta* **2021**, *370*, 137712. [CrossRef]
11. Durst, J.; Siebel, A.; Simon, C.; Hasch'e, F.; Herranz, J.; Gasteiger, H.A. New insights into the electrochemical hydrogen oxidation and evolution reaction mechanism. *Energy Environ. Sci.* **2014**, *7*, 2255. [CrossRef]
12. Cong, Y.; Yi, B.; Song, Y. Hydrogen oxidation reaction in alkaline media: From mechanism to recent electrocatalysts. *Nano Energy* **2018**, *44*, 288–303. [CrossRef]
13. Campos-Roldán, C.A.; Alonso-Vante, N. The Hydrogen Oxidation Reaction in Alkaline Medium: An Overview. *Electrochem. Energy Rev.* **2019**, *2*, 312–331. [CrossRef]
14. Zheng, J.; Nash, J.; Xu, B.; Yan, Y. Towards establishing apparent hydrogen binding energy as the descriptor for hydrogen oxidation/evolution reactions. *J. Electrochem. Soc.* **2018**, *165*, H27–H29. [CrossRef]
15. Campos-Roldán, C.A.; Alonso-Vante, N. Understanding the oxophilic effect on the hydrogen electrode reaction through PtM nanostructures. *J. Solid State Electrochem.* **2021**, *25*, 187–194. [CrossRef]
16. Strmcnik, D.; Uchimura, M.; Wang, C.; Subbaraman, R.; Danilovic, N.; van der Vliet, D.; Paulikas, A.P.; Stamenkovic, V.R.; Markovic, N.M. Improving the hydrogen oxidation reaction rate by promotion of hydroxyl adsorption. *Nat. Chem.***2013**, *5*, 300–306. [CrossRef]
17. Hassan, A.; Carreras, A.; Trincavelli, J.; Ticianelli, E.A. Effect of heat treatment on the activity and stability of carbon supported PtMo alloy electrocatalysts for hydrogen oxidation in proton exchange membrane fuel cells. *J. Power Sources* **2014**, *247*, 712–720. [CrossRef]
18. Gao, J.; Zou, J.; Zeng, X.; Ding, W. Carbon supported nano Pt–Mo alloy catalysts for oxygen reduction in magnesium–air batteries. *RSC Adv.* **2016**, *6*, 83025. [CrossRef]
19. Torres-Santillan, E.; Capula-Colindres, S.; Teran, G.; German, C.M.R.; Flores, M.E.; Valencia, O.G.R. Synthesis of Pt-Mo/WMCNTs nanostructures reduced by the green chemical route and its electrocatalytic activity in the ORR. In *Carbon Nanotubes—Recent Advances, New Perspectives and Potential Applications*; Rahman, M.M., Asiri, A.M.A., Chowdhury, M.A., Eds.; IntechOpen: London, UK, 2022. [CrossRef]
20. Do, C.L.; Pham, T.S.; Nguyen, N.P.; Tran, V.Q.; Pham, H.H. Synthesis and characterization of alloy catalyst nanoparticles PtNi/C for oxygen reduction reaction in proton exchange membrane fuel cell. *Adv. Nat. Sci. Nanosci. Nanotechnol.* **2015**, *6*, 025009.
21. Kong, F.; Ren, Z.; Banis, N.M. Active and Stable Pt–Ni Alloy Octahedra Catalyst for Oxygen Reduction via Near-Surface Atomical Engineering. *ACS Catal.* **2020**, *10*, 4205–4214. [CrossRef]
22. Gu, J.; Zhang, G.-M.; Yao, R.; Yu, T.; Han, M.-F.; Huang, R.-S. High Oxygen Reduction Activity of Pt-Ni Alloy Catalyst for Proton Exchange Membrane Fuel Cells. *Catalysts* **2022**, *12*, 250. [CrossRef]
23. Cheng, X.; Wang, Y.; Lu, Y.; Zheng, L.; Sun, S.; Li, H.; Chen, G.; Zhang, J. Single-atom alloy with Pt-Co dual sites as an efficient electrocatalyst for oxygen reduction reaction. *Appl. Catal. B Environ.* **2022**, *306*, 121112. [CrossRef]
24. Choi, D.S.; Robertson, A.W.; Warner, J.H.; Kim, S.O.; Kim, H. Low-Temperature Chemical Vapor Deposition Synthesis of Pt–Co Alloyed Nanoparticles with Enhanced Oxygen Reduction Reaction. *Catal. Adv. Mater.* **2016**, *28*, 7115–7122. [CrossRef]
25. Wang, X.X.; Hwang, S.; Pan, Y.-T.; Chen, K.; He, Y.; Karakalos, S.; Zhang, H.; Spendelow, J.S.; Su, D.; Wu, G. Ordered Pt3Co Intermetallic Nanoparticles Derived from Metal–Organic Frameworks for Oxygen Reduction. *Nano Lett.* **2018**, *18*, 4163–4171. [CrossRef]
26. Zaman, S.; Su, Y.-Q.; Dong, C.-L.; Qi, R.; Huang, L.; Qin, Y.; Huang, Y.-C.; Li, F.-M.; You, B.; Guo, W.; et al. Scalable Molten Salt Synthesis of Platinum Alloys Planted in Metal–Nitrogen–Graphene for Efficient Oxygen Reduction. *Angew. Chem. Int. Ed.* **2022**, *61*, e202115835. [CrossRef]
27. Zaman, S.; Tian, X.; Su, Y.-Q.; Cai, W.; Yan, Y.; Qi, R.; Douka, A.I.; Chen, S.; You, B.; Liu, H.; et al. Direct integration of ultralow-platinum alloy into nanocarbon architectures for efficient oxygen reduction in fuel cells. *Sci. Bulletin.* **2021**, *66*, 2207–2216. [CrossRef]
28. Ramaswamy, N.; Mukerjee, S. Fundamental Mechanistic Understanding of Electrocatalysis of Oxygen Reduction on Pt and Non-Pt Surfaces: Acid versus Alkaline Media. *Adv. Phys. Chem.* **2012**, *2012*, 491604. [CrossRef]
29. Bogdanovskaya, V.A.; Kuzov, A.V.; Radina, M.V.; Filimonov, V.Y.; Sudarev, G.M.; Osina, M.A. Stability against Degradation and Activity of Catalysts with Different Platinum Load Synthesized at Carbon Nanotubes. *Russ. J. Electrochem.* **2020**, *56*, 969. [CrossRef]

30. Rheinländer, P.J.; Herranz, J.; Durst, J.; Gasteiger, H.A. Kinetics of the Hydrogen Oxidation/Evolution Reaction on Polycrystalline Platinum in Alkaline Electrolyte Reaction Order with Respect to Hydrogen Pressure. *J. Electrochem. Soc.* **2014**, *161*, 1448. [CrossRef]
31. Wang, S.; Lu, A.; Zhong, C.J. Hydrogen production from water electrolysis: Role of catalysts. *Nano Converg.* **2021**, *8*, 4. [CrossRef]
32. Du, C.; Tan, Q.; Yin, G.; Zhang, J. 5—Rotating disk electrode method. In *Rotating Electrode Methods and Oxygen Reduction Electrocatalysts*; Xing, W., Yin, G., Zhang, J., Eds.; Elsevier: Amsterdam, The Netherlands, 2014; pp. 171–198. [CrossRef]